# Differential Rotation in Weakly-Magnetized Neutron Star Atmospheres

## Kristen Menou<sup>1</sup>

<sup>1</sup> Institut d'Astrophysique de Paris, 98bis Boulevard Arago, 75014 Paris, France

14 November 2018

### ABSTRACT

The atmospheres of weakly-magnetized neutron stars expand hydrostatically and rotate differentially during thermonuclear X-ray bursts. Differential rotation is probably related to the frequency drifts of millisecond burst oscillations exhibited by about a dozen nuclear-powered X-ray pulsars. Here, we analyze the linear stability of this differential rotation with respect to local, axisymmetric, multi-diffusive MHD perturbations, at various heights in the neutron star atmosphere. Unstable magneto-rotational modes are identified from within to well above the burning layers. Properties of the fastest growing modes depend sensitively on the local magnetic field geometry. Linear estimates suggest that momentum transport due to magneto-rotational instabilities can affect atmospheric rotation profiles on time-scales relevant to burst oscillations. This transport would likely strengthen the coherence of burst oscillations and contribute to their drifts.

### Key words:

hydrodynamics — MHD — instabilities — turbulence — stars: neutron — stars: rotation — X-rays: bursts

### 1 INTRODUCTION

Since their discovery in the 1970s (see Lewin, van Paradijs & Taam 1995 for a review), thermonuclear X-ray bursts have been observed from a large number of low-mass X-ray binaries containing weakly-magnetized accreting neutron stars. The basic physical mechanism responsible for X-ray bursts, namely mass accumulation on the neutron star surface at rates such that a thermonuclear He or mixed H/He flash is eventually triggered, is well understood (see, e.g., Bildsten 1998 and references therein). The phenomenology of X-ray bursts is rich, however, and theoretical models face some difficulties when detailed comparisons with the observations are attempted (e.g. Bildsten 2000; Galloway et al. 2003).

This situation has become more serious, and more exciting, in the past decade, with the discovery of transient millisecond (300–600 Hz) oscillations during some X-ray bursts, the so-called burst oscillations (Strohmayer et al. 1996). While the presence of oscillations during burst rise may be understood as resulting from the rotational modulation of a nuclear burning spot spreading around the stellar surface (Spitkovsky, Levin & Ushomirsky 2002), it is unclear why oscillations should be visible past the burst peak, when the burning fuel has presumably been entirely ignited. Also intriguing is the nature of frequency drifts exhibited by most burst oscillations (generally spin-ups, by a few Hz at most) and the origin of the diversity they show in terms

of drift time-scales and amplitudes (see Strohmayer & Bild-sten 2003 for a review). Observations of the burst oscillation phenomenon have been very rewarding. In particular, it has recently been shown that the burst oscillation asymptotic frequency (after complete spin-up) and the independently-known neutron star spin frequency are closely related in two millisecond accreting pulsars (Chakrabarty et al. 2003; Strohmayer et al. 2003). Still, our understanding of the physical mechanisms involved in burst oscillations and associated frequency drifts remains limited.

Following Strohmayer et al. (1997), Cumming & Bildsten (2000) proposed that frequency drifts originate from the rotational evolution of heated burning layers, as they cool, hydrostatically contract and nearly recover their original rotation, assuming their specific angular momentum is conserved at all times. These same authors later realized, however, that the largest observed frequency drifts are in excess of the amplitudes expected in their burning layer scenario, by as much as a factor 2-3. Apparently, only layers higher up in the atmosphere would have the right amount of rotational offset to explain the largest drift amplitudes (Cumming et al. 2002). More recently, Chakrabarty et al. (2003) have also argued that the very rapid drift (spin-up) that they have observed during the rise phase of one of the bursts of SAX J1808-3658 effectively rules out the scenario of Cumming & Bildsten (2000). There is currently no solid alternative explanation for the origin of burst oscillations and associated frequency drifts, even though both Rossby wave (Heyl 2003; but see Lee 2003) and zonal flow (Spitkovsky et al. 2002) scenarios have been proposed.

In their study of neutron star atmospheres, Cumming & Bildsten (2000) have analyzed a number of mechanisms which could make the vertical differential rotation established via burst-induced hydrostatic expansion unstable. They have not identified any clear destabilizing process (which would presumably lead to angular momentum transport between atmospheric shells) and this was the main motivation for their assumption of conserved specific angular momentum. The purpose of the present study is to reconsider the issue of stability of differential rotation in the atmospheres of weakly-magnetized, rapidly-rotating neutron stars.

As noted by Cumming & Bildsten (2000), the strong vertical thermal stratification of a neutron star atmosphere stabilizes it with respect to adiabatic perturbations, even in the presence of strong vertical differential rotation. Although not considered by these authors in their analysis, one indeed verifies that the vertical differential rotation expected in the present context is stable according to both the hydrodynamical Solberg-Høiland adiabatic criteria (e.g. Tassoul 1978) and their generalization for weakly-magnetized fluids (Balbus 1995).

This situation is reminiscent of the solar radiative interior, where thermal stratification also plays a strongly stabilizing role. Goldreich & Schubert (1967) and Fricke (1968) have shown, however, that rotational instabilities can still exist, provided perturbed fluid elements are allowed to exchange heat with their environment much faster than they exchange momentum. The stabilizing role of the atmospheric thermal stratification is then effectively neutralized when a perturbed fluid element reaches thermal equilibrium with its environment while its original momentum remains largely unchanged. In the solar interior, radiative heat diffusion is indeed orders of magnitude faster than viscous diffusion of momentum, and this was the initial motivation for the double-diffusive analysis of Goldreich & Schubert and Fricke (hereafter GSF altogether). The basic doublediffusive mechanism invoked in these instabilities is not too different from that of "salt-finger" instabilities operating in the Earth's oceans, except that the destabilizing salinity stratification is replaced by a destabilizing angular momentum stratification in the stellar context.

As we shall see below, conditions in the atmospheres of weakly-magnetized neutron stars during bursts are also strongly multi-diffusive. It is then possible that rotational instabilities will develop and affect the differentially-rotating atmospheric layers in such a way as to influence the observational properties of burst oscillations. To address this question properly, it is necessary to account for the presence of magnetic fields in neutron star atmospheres. Recently, Menou, Balbus & Spruit (2004) have generalized the work of GSF to weakly-magnetized fluids. They have shown that the combination of weak magnetic fields and a multi-diffusive situation may have contributed to establishing the state of near solid-body rotation inferred from helioseismology for the solar interior.

In this paper, we present a specific application of the stability analysis of Menou et al. (2004) to weaklymagnetized, differentially-rotating neutron star atmospheres and we discuss possible consequences for the phenomenology of burst oscillations and associated frequency drifts. We describe our method of solution in §2. In §3, we present the results of our stability analysis at various heights in the neutron star atmosphere. The relevance of these results to burst oscillations is discussed in §4.

### 2 METHOD

Following Menou et al. (2004), we perform a local, linear stability analysis of differential rotation in a weakly-magnetized, stably-stratified fluid. In this section, we first recall the dispersion relation obeyed by axisymmetric modes in a general context in §2.1. We describe how this dispersion relation can be applied to the specific problem of weakly-magnetized neutron star atmospheres during bursts in §2.2. We then describe how we obtained numerical solutions to the dispersion relation in §2.3. In §2.4, we discuss the issue of the efficiency of momentum transport, that we estimate from linear mode properties. Our basic analysis follows closely that presented in Menou et al. (2004), where additional details on the method can be found.

### 2.1 Dispersion Relation

We initially work in cylindrical coordinates,  $(R, \phi, Z)$ , but we will also later express results in terms of spherical coordinates,  $(r, \theta, \phi)$ . We consider axisymmetric Eulerian perturbations with a WKB space-time dependence  $\exp[i(\mathbf{k} \cdot \mathbf{r} - \omega t)]$ , where  $\mathbf{k} = (k_R, 0, k_Z) = (k_r, k_\theta, 0)$ . Starting from the set of MHD equations (continuity, momentum, induction, energy) that include the effects of viscosity, resistivity and heat conduction

$$\frac{\partial \rho}{\partial t} + \nabla \cdot (\rho v) = 0, \tag{1}$$

$$\rho \frac{\partial \mathbf{v}}{\partial t} + (\rho \mathbf{v} \cdot \nabla) \mathbf{v} = -\nabla \left( P + \frac{B^2}{8\pi} \right) - \rho \nabla \Phi + \left( \frac{B}{4\pi} \cdot \nabla \right) B + \mu \left( \nabla^2 \mathbf{v} + \frac{1}{3} \nabla (\nabla \cdot \mathbf{v}) \right), \tag{2}$$

$$\frac{\partial \boldsymbol{B}}{\partial t} = \boldsymbol{\nabla} \times (\boldsymbol{v} \times \boldsymbol{B}) - \eta \boldsymbol{\nabla} \times (\boldsymbol{\nabla} \times \boldsymbol{B}), \qquad (3)$$

$$\frac{1}{(\gamma - 1)} P \frac{d \ln P \rho^{-\gamma}}{dt} = \chi \nabla^2 T, \tag{4}$$

one derives, under the Boussinesq approximation and ignoring self-gravity, the following fifth-order dispersion relation for local, axisymmetric, multi-diffusive modes,

$$\widetilde{\omega}_{b+v}^{4} \omega_{e} \frac{k^{2}}{k_{Z}^{2}} + \widetilde{\omega}_{b+v}^{2} \omega_{b} \left[ \frac{1}{\gamma \rho} (\mathcal{D}P) \mathcal{D} \ln P \rho^{-\gamma} \right]$$

$$+ \widetilde{\omega}_{b}^{2} \omega_{e} \left[ \frac{1}{R^{3}} \mathcal{D}(R^{4} \Omega^{2}) \right] - 4 \Omega^{2} (\mathbf{k} \cdot \mathbf{v}_{A})^{2} \omega_{e} = 0,$$
 (5)

where

$$v_A = B/\sqrt{4\pi\rho}, \qquad k^2 = k_R^2 + k_Z^2,$$

$$\begin{split} \widetilde{\omega}_{b+v}^2 &= \omega_b \omega_v - (\boldsymbol{k} \cdot \boldsymbol{v_A})^2, \qquad \widetilde{\omega}_b^2 = \omega_b^2 - (\boldsymbol{k} \cdot \boldsymbol{v_A})^2, \\ \omega_b &= \omega + i \eta k^2, \qquad \omega_v = \omega + i \nu k^2, \\ \omega_e &= \omega + \frac{\gamma - 1}{\gamma} \frac{i T}{P} \chi k^2, \qquad \mathcal{D} \equiv \left(\frac{k_R}{k_Z} \frac{\partial}{\partial Z} - \frac{\partial}{\partial R}\right). \end{split}$$

A developed form of the dispersion relation can be found in Menou et al. (2004). The Brunt-Väisälä frequency, N, which measures the magnitude of atmospheric thermal stratification, comes out of the first bracket term above. Similarly, the epicyclic frequency, which measures the angular momentum "stratification," comes out of the second bracket term. The notation is standard and identical to that adopted in Menou et al. (2004):  $\boldsymbol{v}$  is the fluid velocity,  $\rho$  is the mass density, P is the pressure,  $\Phi$  is the gravitational potential, T is the temperature,  $\boldsymbol{B}$  is the magnetic field,  $\mu$  is the dynamic viscosity,  $\nu = \mu/\rho$  is the kinematic viscosity,  $\eta$  is the resistivity,  $\chi$  is the heat conductivity and  $\boldsymbol{v}_{\boldsymbol{A}}$  is the Alfvén speed.

A value  $\gamma = 5/3$  is adopted for the gas adiabatic index and a perfect gas equation of state is assumed. Models of neutron star atmospheres during thermonuclear X-ray bursts show that radiation pressure sometimes contribute a non-negligible fraction to the total pressure, especially close to the burning layers (see, e.g., Cumming & Bildsten 2000). We neglect this contribution here, but it should be included for better accuracy. Degeneracy is neglected, because it is lifted during bursts, and general relativistic effects are ignored. When discussing burning layers, we also ignore the effects that any remaining nuclear burning may have on stability, both as a heat source and in modifying the composition of burning regions. The basic state rotation is given by  $\Omega = (0, 0, \Omega(R, Z))$  along the Z-axis. The basic state magnetic field, whose geometry is specified below, is assumed to be weak with respect to both rotation and thermal pressure.

### 2.2 Neutron Star Atmosphere During Burst

In order to solve the above dispersion relation (Eq. [5]), we must specify values for all the physical parameters entering the problem. Often, we rely on the recent, one-dimensional, hydrostatic models of Cumming & Bildsten (2000) for neutron star atmospheres during bursts. We consider conditions in three representative layers, right after burst trigger and the hydrostatic expansion that follows it. The first such layer, labeled "Burning" in Table 1, is representative of conditions in the burning layers. The second layer, labeled "High", corresponds to typical conditions high in the atmosphere, well above the burning layers but still well below the stellar photosphere (conditions provided by A. Cumming, private communication). The third layer, labeled "Middle", corresponds to atmospheric conditions intermediate between the first two. Our choice of layers, although somewhat arbitrary, will prove to be useful to illustrate variations of the stability properties with height in the neutron star atmosphere. We list in Table 1 the values of the density,  $\rho$ , temperature, T, and Rosseland-mean radiative opacity,  $\kappa$  (from electron scattering), in the three layers of interest.

We need to estimate the values of various microscopic diffusion coefficients relevant to the stability problem. From Spitzer (1962) and Schwarzschild (1958), assuming that the plasma is mostly composed of hydrogen, the (ion-dominated) dynamic viscosity,  $\mu$ , the radiative kinematic

viscosity,  $\nu_r$ , the electric resistivity,  $\eta$ , the radiative heat conductivity,  $\chi_{rad}$ , and the corresponding heat diffusivity,  $\xi_{rad}$ , are given by

$$\mu = \rho \nu \simeq 2.2 \times 10^{-15} \frac{T^{5/2}}{\ln \Lambda} \text{ g cm}^{-1} \text{ s}^{-1},$$
 (6)

$$\nu_r = \frac{16}{15} \frac{\sigma T^4}{\kappa \rho^2 c^2} \text{ cm}^2 \text{ s}^{-1}, \tag{7}$$

$$\eta \simeq 5.2 \times 10^{11} \frac{\ln \Lambda}{T^{3/2}} \text{ cm}^2 \text{ s}^{-1},$$
(8)

$$\chi_{rad} = \frac{16T^3\sigma}{3\kappa\rho} \text{ c.g.s.}, \tag{9}$$

$$\xi_{rad} = \frac{\gamma - 1}{\gamma} \frac{T}{P} \chi_{rad} \text{ cm}^2 \text{ s}^{-1}, \qquad (10)$$

where  $\ln \Lambda$  is the Coulomb logarithm, c is the speed of light and  $\sigma$  is the Stefan-Boltzmann constant. We list in Table 1 the values of all three diffusivity coefficients for the three layers of interest. In addition, the values of the Prandtl number,  $\epsilon_{\nu} = \nu_{\rm tot}/\xi_{rad} = (\nu + \nu_r)/\xi_{rad}$ , and the "Acheson number,"  $\epsilon_{\eta} = \eta/\xi_{rad}$ , which together measure the hierarchy of diffusive processes, are listed. Viscous diffusion clearly dominates over resistive diffusion in the neutron star atmosphere (a situation which is opposite to that in the Sun's radiative interior; Menou et al. 2004), but radiative heat diffusion is the strongest by many orders of magnitude (as is the case for the solar interior). It is this property of rapid heat diffusion that allows multi-diffusive modes to overcome the stabilizing influence of the atmospheric thermal stratification. Note also how the situation becomes more doublediffusive as one goes up in the atmosphere (since the values of  $\epsilon_{\nu}$  and  $\epsilon_{\eta}$  decrease), and how radiative viscosity eventually dominates over ion viscosity high enough above the burning layers.

A number of global parameters for the magnetized, differentially-rotating neutron star atmosphere must be specified. We adopt a value  $\Omega=2\times 10^3~{\rm s}^{-1}$  for the neutron star angular velocity, corresponding to a typical spin period of  $\sim 3~{\rm ms}$  (spin frequency  $\sim 300~{\rm Hz}$ ). We adopt a value  $N/\Omega \simeq 10^2$  for the ratio of the Brunt-Väisälä frequency to the angular velocity (Cumming & Bildsten 2000). Note that we only include the thermal stratification in our definition of the Brunt-Väisälä frequency since the dispersion relation that we are solving was derived ignoring the effects of composition gradients. The issue of stabilization due to composition gradients is important and is further discussed in §4.

We need to specify the level of differential rotation present in the atmosphere. After burst trigger, all the atmospheric layers, from the burning regions to those located higher up, are heated up. This occurs on a thermal timescale, which is much in excess of a local sound crossing time (Cumming & Bildsten 2000) and, as a result, the layers expand hydrostatically. Assuming conservation of specific angular momentum during this phase, differential rotation between spherical shells should then be established at a level corresponding to  $\partial \ln \Omega/\partial \ln r = -2$ , in all three layers of interest. We further assume that no differential rotation is present within spherical shells. It should be noted that any such negative differential rotation (i.e.  $\partial \ln \Omega/\partial \theta < 0$ ) would

Layer	$(g \text{ cm}^{-3})$	$T (10^8 \text{ K})$	$(\operatorname{cm}^2\operatorname{g}^{-1})$	$(\operatorname{cm}^2\operatorname{s}^{-1})$	$(\operatorname{cm}^2 \operatorname{s}^{-1})$	$(\operatorname{cm}^2 \operatorname{s}^{-1})$	$\begin{array}{c} \xi_{rad} \\ (\text{cm}^2 \text{ s}^{-1}) \end{array}$	$\epsilon_{ u} \ ( u_{ m tot}/\xi_{rad})$	$rac{\epsilon_{\eta}}{(\eta/\xi_{rad})}$
Burning Middle High	$   \begin{array}{c}     10^5 \\     3 \times 10^3 \\     100   \end{array} $	10 5 2	0.15 0.17 0.23	$   \begin{array}{c}     88 \\     680 \\     2.1 \times 10^{3}   \end{array} $	$34 \\ 2.5 \times 10^3 \\ 4.4 \times 10^4$	0.13 0.28 1.1	$4.5 \times 10^{5}$ $5.6 \times 10^{7}$ $2.4 \times 10^{9}$	$2.7 \times 10^{-4}$ $5.7 \times 10^{-5}$ $1.9 \times 10^{-5}$	$2.9 \times 10^{-7}$ $5 \times 10^{-9}$ $4.6 \times 10^{-10}$

Table 1. Typical Atmospheric Conditions During Burst

be unstable to adiabatic magneto-rotational modes (Balbus 1995; Menou et al. 2004).

Finally, we must specify a geometry and a strength for the basic state magnetic field present in the atmospheric layers. Although other configurations are possible (for instance with high multipoles; see also Ruderman 2003), we will assume here, for simplicity, a misaligned dipole geometry. More precisely, because our analysis is axisymmetric in nature, we must use an "axisymmetric dipole" geometry, which best resembles that of a true dipole. The sphericalradial and polar components of the field are thus

$$B_r = B_p \cos(\theta - \theta_{\text{mis}}), \quad B_\theta = \frac{B_p}{2} \sin(\theta - \theta_{\text{mis}}),$$
 (11)

where  $\theta$  is the polar angle ( $\theta = 0$  or  $\pi$  on the neutron star rotation axis),  $\theta_{\rm mis}$  is the equivalent of the angle by which the dipolar magnetic axis is misaligned from the rotation axis and  $B_n$  is the polar field strength at the neutron star surface (assumed to be the same in all layers of interest). With this geometry, field lines have an axisymmetric configuration such that they are nearly vertical for angles  $\theta \sim \theta_{\rm mis}$  (magnetic "pole," which is an axisymmetric band, really) and nearly horizontal at the magnetic equator. This setup allows us to study the effects of the magnetic field geometry on the stability properties. We have investigated stability in the three atmospheric layers of interest for values of  $B_p$  ranging from  $10^7$  to  $10^9$  G, considered as typical for weakly-magnetized accreting neutron stars.

#### 2.3Numerical solutions

The complexity of the dispersion relation (Eq. [5]) makes it difficult to analytically derive necessary and sufficient conditions for stability (Menou et al. 2004). In addition, since we are interested in studying the properties of unstable modes, we want to solve the dispersion relation numerically, with the appropriate set of parameters. To do this, we use the Laguerre algorithm described by Press et al. (1992) to solve equation (5) as a fifth-order complex polynomial for  $\sigma = -i\omega$ , with real coefficients.

We have found useful to rewrite both the rotational and thermal stratification bracket terms appearing in the dispersion relation in spherical coordinates  $(r, \theta, \phi)$ . The thermal stratification term then becomes function only of  $N^2$ ,  $\theta$  and the radial and angular wavevectors,  $k_r$  and  $k_\theta$ , for a spherically symmetric star. The rotational stratification term, on the other hand, explicitly depends on the amount of differential rotation within and between spherical shells, that we express as  $\partial \ln \Omega / \partial \theta$  and  $\partial \ln \Omega / \partial \ln r$ , respectively. As we have mentioned earlier, we are interested here in the specific case corresponding to  $\partial \ln \Omega / \partial \theta = 0$  and  $\partial \ln \Omega / \partial \ln r = -2$ .

For each of the three atmospheric layers of interest, we search for unstable modes (which correspond to  $\sigma$ -roots with positive real parts) at various locations on the stellar sphere. We consider values of the polar angle,  $\theta$ , in the range  $0 \to \pi/2$  (pole to equator). At each location, we perform a search for unstable modes by varying the wavevectors  $k_r$  and  $k_{\theta}$  independently in the range  $\pm [2\pi/l_{\rm max}, 2\pi/l_{\rm min}]$ . The first, large-scale limit,  $l_{\text{max}}$ , is chosen to be  $\lesssim H$ , the pressure scale height, so that the local and weak field assumptions of our analysis remain valid. The second, small-scale limit,  $l_{\min}$ , is chosen to be  $\gg \lambda$ , the mean free path, so that the analysis remains valid given our use of fluid equations. We estimate  $H \simeq \Re T/g$ , where  $\Re$  is the perfect gas constant,  $\lambda \sim \nu/\sqrt{\Re T}$ and we use  $g \simeq 2 \times 10^{14} \text{ cm s}^{-2}$  as a typical neutron star surface gravity. In addition, we systematically perform focused searches in regions of the wavevector space corresponding to nearly cylindrical-radial displacements ( $|k_R/k_Z| \rightarrow 0$ ) and nearly vertical displacements  $(|k_R/k_Z| \to \infty)$ .

#### **Efficiency of Transport** 2.4

The differential rotation established in neutron star atmospheres during bursts is an intrinsically transient phenomenon. Absent any transport mechanism, the various differentially-rotating spherical shells would essentially recover their original rotation (modulo a small offset due to changes in molecular weight; Cumming & Bildsten 2000) once the atmosphere cools down to pre-burst conditions, typically after several tens of seconds. In the presence of a transport mechanism, however, the issue of the efficiency of momentum transport is of direct relevance to the observations because a mechanism effective enough to act on timescales of tens of seconds or shorter would influence the rotational evolution of atmospheric layers during burst.

It is unclear whether one can determine, from a linear analysis only, the efficiency of transport that would result from non-linear growth and turbulence. We will adopt an often-used prescription here, by assuming that the efficiency of transport can be crudely estimated from the growth rate and length-scale of the fastest-growing unstable linear mode. There is no general justification for this simple prescription, except perhaps examples of physical situations for which it is not too far off (for instance, the emergence of midlatitude weather structures in the Earth's turbulent atmosphere with sizes matching linear predictions for the fastest growing baroclinic modes is considered a success of baroclinic theory; see Pedlosky 1987). Our goal here is not to accurately estimate the efficiency of momentum transport between shells, but merely to question the observational relevance of this transport given typical burst durations.

It should be noted that the non-linear numerical simulations of Korycansky (1991) lend support to the simple prescription we adopted. This author found, for an equatorial setup (i.e. aligned thermal and angular momentum stratifications), that the non-linear behavior of hydrodynamical double-diffusive (GSF) modes is well described by a combination of linear growth rate and spherical-radial length scale of the instability. Assuming this property carries over to magnetized modes and to other geometries (i.e. away from the stellar equator), we will be estimating the efficiency of momentum transport across spherical shells with the quantity  $\sigma_{\text{max}}/(k_r^2)_{\text{max}}$  (dimension of a viscosity), where  $\sigma_{\text{max}}$  is the growth rate of the fastest-growing mode and  $(k_r)_{\text{max}}$ is the spherical-radial wavevector component of that same mode. Clearly, using linear theory to predict a non-linear outcome is a daring extrapolation, so one should treat our results on transport efficiencies with much caution.

### 3 RESULTS

For each of the three atmospheric layers of interest, we have run several models to identify parameter dependencies. To best illustrate these dependencies, we have chosen a specific subset of models, listed in Table 2. In most cases, only the magnetic field strength,  $B_p$ , or the value of  $\theta_{\rm mis}$ , the angle by which the magnetic "pole" is misaligned from the rotation axis, are varied. But we also show the effects of variations in the neutron star rotation rate,  $\Omega$ , the rate of spherical-radial differential rotation,  $\partial \ln \Omega / \partial \ln r$ , and the maximum allowed scale for perturbations.

Quite generally, many unstable modes were found in the searched wavevector space, as expected for the strongly multi-diffusive conditions considered. All the unstable modes that we have identified were of the "direct" type (i.e. with  $Im(\sigma) = 0$ ), as opposed to the other multidiffusive "overstable" type (when  $|Im(\sigma)| > Re(\sigma) > 0$ ). This is a consequence of the strongly stabilizing thermal stratification and of the fast rate of heat diffusion (relative to momentum diffusion), as was the case for the solar radiative zone (Menou et al. 2004). To simplify the description of these unstable modes, we focus our attention on the properties of the fastest-growing mode identified, as a function of location on the stellar sphere (i.e. polar angle,  $\theta$ ). While we cannot guarantee that we have identified the single fastest-growing mode at any location, convergence tests with increasingly higher resolutions for the wavevector grid and the polar angle grid were successfully passed, suggesting that our search method is robust. It is worth pointing out that we have often experienced unsatisfactory numerical convergence for small values of the polar angle, i.e.  $\theta \sim 0$  (close to the rotation axis). This may be caused by the condition for a weak magnetic field compared to rotation becoming increasingly more stringent at small  $\theta$  values (where pressure gradients become nearly orthogonal to the centrifugal force), but we have not explored this possibility further. We also do not explicitly show results for a magnetic field strength  $B_p = 10^9$  G. For reasons that will become clear by the end of this section,

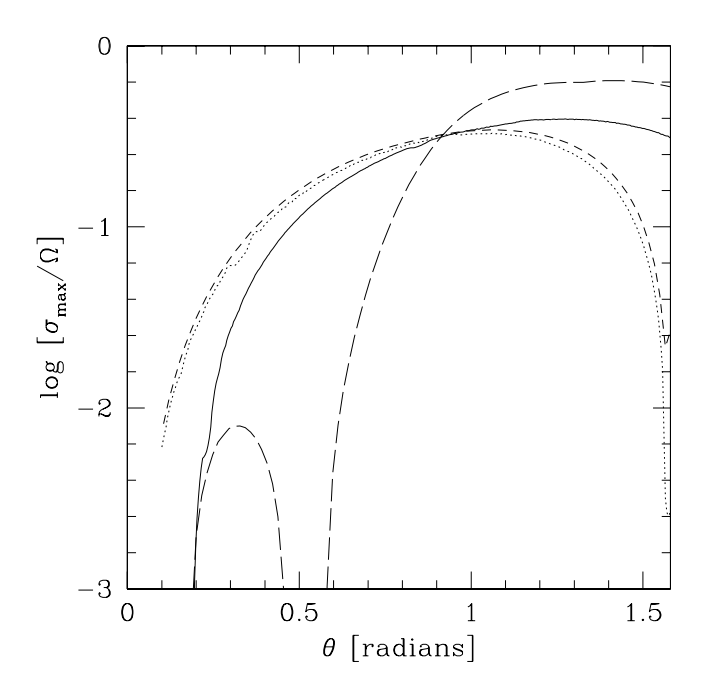


**Figure 1.** Growth rate of the fastest-growing mode,  $\sigma_{\rm max}$ , in units of angular velocity,  $\Omega$ , as a function of polar angle,  $\theta$  (rotational equator at  $\theta = \pi/2$ ). The solid, dotted, short-dashed and long-dashed lines correspond to models B3, B1, B2 and H1 in Table 2, respectively.

searches for unstable modes in this stronger field situation have been unsuccessful high in the atmosphere.

We begin with a discussion of the general properties of fastest-growing unstable modes identified in the burning layers, before comparing them with the properties of fastestgrowing modes identified higher-up in the atmosphere.

### 3.1 Burning Layers

Figure 1 shows the maximum growth rate among all unstable modes, in units of the neutron star angular velocity,  $\Omega$ , as a function of polar angle,  $\theta$ . The solid, dotted and short-dashed lines correspond to models B3, B1 and B2 in Table 2, respectively. These models differ in the strength of the magnetic field and by how much the magnetic "pole" is misaligned from the rotation axis at  $\theta = 0$ .

In all three models, the growth rate of the fastest-growing mode is a function of polar angle,  $\theta$ , which shows that the combination of magnetic field and stellar spherical geometries have an influence on stability properties. The similarity between the dotted and short-dashed lines also indicates that the magnetic field strength does not strongly affect growth rates, although we will see later that it does matter in a global sense (§3.2). On the other hand, there is a clear distinction between the solid line (model B3) and the dotted and short-dashed lines, indicating that the magnetic field geometry alone influences the stability properties quite a lot.

These trends are confirmed by looking at the wavenumber properties of the same modes. Figure 2 shows the ratio of spherical-radial to polar wavenumber,  $|k_r/k_\theta|$ , for the fastest-growing modes, as a function of polar angle,  $\theta$ . The

Model	Layer	$\frac{\partial \ln \Omega}{\partial \ln r}$	$B_p$ (Gauss)	$\theta_{ m mis}$ (degrees)	Special
			0		_
B1	Burning	-2	$10^{8}$	0	
$_{ m B2}$	Burning	-2	$10^{7}$	0	
В3	Burning	-2	$10^{8}$	30	
M1	Middle	-2	$10^{8}$	30	
M2	Middle	-2	$10^{8}$	0	
M3	Middle	-2	$10^{8}$	20	
M4	Middle	-2	$10^{8}$	30	$\Omega  imes 2$
		_			
H1	High	-2	$10^{7}$	30	
H2	High	-1	$10^{7}$	30	
	_	$-1 \\ -2$	$10^{7}$		1 1 D
Н3	$_{ m High}$	-2	10.	30	large $l_{\rm max} \sim R_{\rm NS}$

Table 2. Models and Parameters

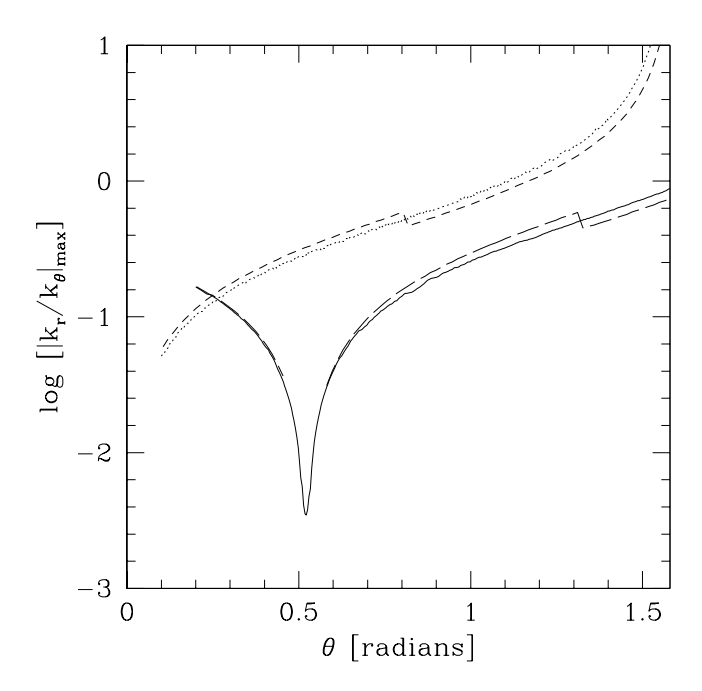


**Figure 2.** Ratio of spherical-radial to polar wavenumber,  $|k_r/k_\theta|$ , for the fastest-growing mode, as a function of polar angle,  $\theta$ . Notation is identical to Fig. 1, for the same four models (solid: B3; dotted: B1; short-dashed: B2; long-dashed: H1).

notation is identical to Figure 1, for ease of comparison. Once again, the magnetic field strength is found to have little influence on the mode properties, but the magnetic field and stellar spherical geometries do. <sup>1</sup>

Figure 2 reveals an interesting wavenumber property

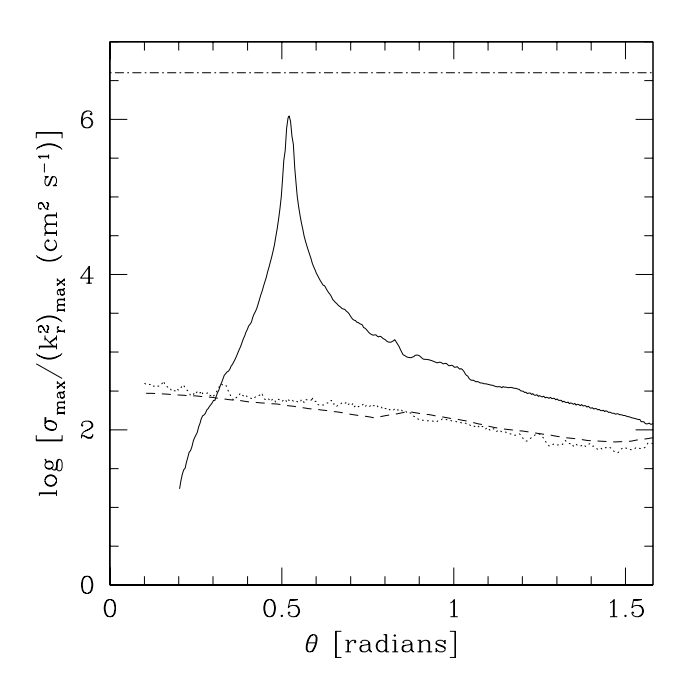
of fastest-growing modes. In the two models with a magnetic dipole aligned with the rotation axis, the nature of the modes changes from mostly spherical-radial  $(|k_r/k_\theta| \ll 1)$ for small  $\theta$  values to mostly horizontal  $(|k_r/k_\theta| \gg 1)$  as one approaches the stellar equator  $(\theta \to \pi/2)$ . In the model with a magnetic "pole" misaligned by  $\theta_{\rm mis} = 30$  deg, on the other hand,  $|k_r/k_\theta|$  is  $\ll 1$  on a fair fraction of the stellar sphere, although it approaches unity at the stellar equator. This behavior can be understood as resulting mostly from the magnetic field geometry. At the magnetic "poles," where the field is nearly spherical-radial, the fastest-growing mode tends to be nearly spherical-radial itself, with  $|k_r/k_\theta| \ll 1$ . As one approaches the magnetic equator, however, the field becomes nearly horizontal and so does the fastest-growing mode. This is consistent with a tendency for the fastestgrowing mode to minimize the amount of magnetic tension it is subject to, by favoring displacements nearly along field lines.

Figure 3 shows estimates of the efficiency of momentum transport in the spherical-radial direction, based on fastestgrowing linear mode properties, as a function of polar angle  $\theta$ . Again, notation is similar to that in Figs. 1 and 2 for models B1 (dotted line), B2 (dashed line) and B3 (solid line). In model B3, which corresponds to a misaligned magnetic dipole, the estimated efficiency of transport is strongly peaked at the magnetic "pole" (because of a significant increase of the mode radial wavelength, as we shall see below and in Fig. 6). The horizontal dash-dotted line in Figure 3 indicates the efficiency typically required in the burning layers to affect the rotation profile over a local pressure scaleheight,  $H \simeq \Re T/g$ , in 1 second. This reference efficiency was simply calculated as  $H^2$  cm<sup>2</sup> s<sup>-1</sup>. It would not make much sense to calculate a reference efficiency for a lengthscale exceeding H because both atmospheric and stability

growing mode with local geometry). We have not investigated this further

<sup>&</sup>lt;sup>1</sup> We have checked that the discontinuities present in the shortand long-dashed lines in figure 2, and absent from the corresponding growth rates in figure 1, persist even at higher wavenumber or polar angle grid resolutions. Consequently, they appear to have a physical origin (possibly a change in the nature of the fastest-

<sup>&</sup>lt;sup>2</sup> The nearly incompressible modes described by our dispersion relation are characterized by displacements orthogonal to the mode wavevector, k.



**Figure 3.** Estimate of the efficiency of spherical-radial momentum transport,  $\sigma_{\rm max}/k_r^2$  (dimension of a viscosity), based on fastest-growing mode properties in typical burning layer conditions, as a function of polar angle,  $\theta$ . The solid, dotted and dashed lines correspond to models B3, B1 and B2 in Table 2, respectively. The location of the magnetic "pole" at  $\theta=30$  deg in model B3 is obvious. The horizontal dash-dotted line indicates the efficiency required to affect the rotation profile over a local scale-height in 1 s.

conditions start to change significantly over a local pressure scale-height.

Interestingly, the maximum momentum transport efficiency estimated from fastest-growing mode properties, at the magnetic "pole," falls short of the reference efficiency only by a factor of a few, suggesting that several seconds may be sufficient for the rotational profiles to be affected. Away from the magnetic "pole" (and essentially everywhere on the stellar sphere in aligned-dipole models B1 and B2), estimated transport efficiencies appear too small, by several orders of magnitude, to affect rotation profiles over a local scale-height on observationally relevant time-scales. In fact, the efficiencies indicated by the dashed and dotted lines in Figure 3 are small enough to be comparable to that of microscopic viscosity  $(\nu + \nu_r)$  in the burning layers, as can be seen from Table 2.

Many of the basic properties we have just described for fastest-growing modes in burning layers carry over to higher atmospheric layers. There are important differences, however, that we will now illustrate. Rather than going through a description of growth rates and wavenumbers independently for all cases of interest, we will often summarize results by focusing on transport efficiencies (which are a combination of the two) and how these are affected by changes in physical conditions higher up in the atmosphere.

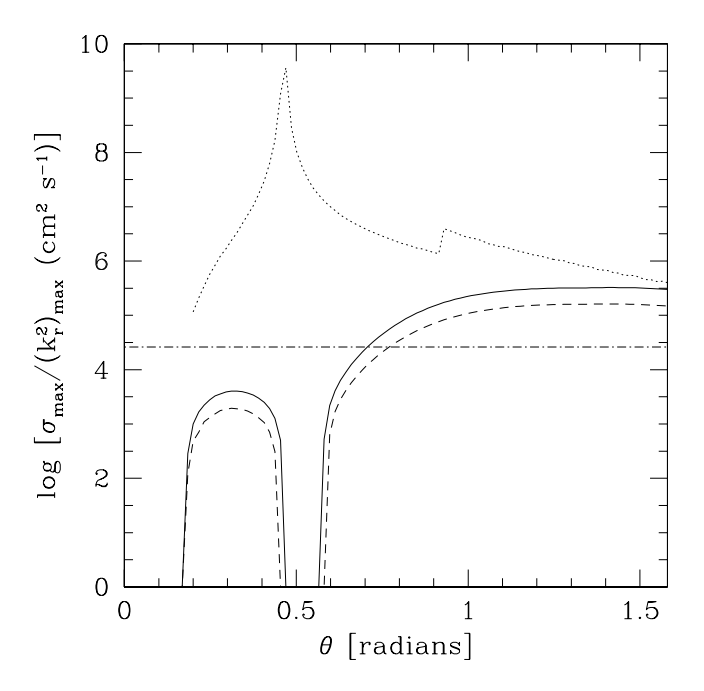


Figure 4. Estimate of the efficiency of spherical-radial momentum transport for typical conditions in a high-atmospheric layer, as a function of polar angle,  $\theta$ . The solid, dotted and dashed lines correspond to models H1, H3 and H2 in Table 2, respectively. The horizontal dash-dotted line indicates the efficiency required to affect the rotation profile over a local scale-height in 1 s.

### 3.2 High Atmosphere

In addition to the three burning layer models we have already discussed, figures 1 and 2 show, as long-dashed lines, the growth rates and wavenumber properties of fastest-growing modes in our fiducial model for a high atmospheric layer (model H1 in Table 2). Although strong similarities exist between models H1 and B1 (solid line), especially in terms of wavenumber properties, a striking difference is the absence of any unstable mode in the vicinity of the magnetic "pole," at  $\theta \sim 30$  deg. As we shall see, this results from the length-scale of potentially unstable modes exceeding the maximum value allowed by our search,  $l_{\rm max} \sim H$  (the local scale height).

Figure 4 shows estimates of the efficiency of momentum transport in the spherical-radial direction, based on fastest-growing linear mode properties in the high atmospheric layer, as a function of polar angle  $\theta$ . The solid, dotted and dashed lines correspond to models H1, H3 and H2, respectively. The horizontal dash-dotted line indicates again the efficiency typically required to affect the rotation profile over a local scale height in 1 s ( $\sim H^2 \text{ cm}^2 \text{ s}^{-1}$ ).

Model H3 (dotted line) is voluntarily artificial, in that it allows the length-scale of unstable modes to be as large as the neutron star radius,  $R_{\rm NS}$  (taken to be 10 km), rather than the local scale-height of the high-atmospheric layer,  $H \sim 150$  cm. The efficiency of momentum transport in this artificial model is strongly peaked around the magnetic "pole," at  $\theta \sim 30$  deg, and much resembles that of model B3 (solid line in Fig. 3). Clearly then, the difference with model H1, and in particular the absence of any unstable

mode in the vicinity of the magnetic "pole," results from the tendency of these modes to have large length-scales, in excess of  $l_{\rm max} \sim H$ , for typical conditions high-up in the atmosphere.

This property is consistent with the gradual breakdown, as one goes up in the atmosphere, of the important weakfield assumption made in our analysis. Indeed, while the magnetic field strength may not vary significantly over a few scale heights, density and pressure do. As a result, our working hypothesis of a magnetic field weak compared to thermal pressure becomes increasingly difficult to satisfy. Specifically, while the Alfvén speed,  $v_A \propto B\rho^{-1/2}$ , increases in the more tenuous high atmosphere, the sound speed,  $c_S \propto T^{1/2}$ , decreases and the requirement  $v_A \ll c_S$  becomes less and less valid. It is only marginally satisfied in the highatmospheric layer we have considered  $(v_A/c_S \sim 0.1)$  for the values of  $B_p$  adopted) and this is the origin of the disappearance of unstable modes around the magnetic "pole" in model H1 (e.g. Fig. 4). While large-scale displacements subject to weak enough magnetic tension for instability could be found in principle, they are clearly outside the regime of validity of our weak-field analysis. Even higher up in the atmosphere, the weak field regime breaks down completely and all unstable diffusive magneto-rotational modes disappear.

Still, some of the fastest-growing modes identified in our realistic high-atmosphere H1 model (solid line in Fig. 4) could affect rotation profiles over a local scale height on rather short time-scales, especially near the stellar equator. Provided that these unstable modes act to reduce the amount of differential rotation initially present, a rotational recoupling of unstable layers in the high atmosphere would then be expected on observationally interesting time-scales. It is important to notice, however, that the magnitude of microscopic viscosity  $(\nu + \nu_r)$  in high-atmospheric layers (compare Table 1 and Fig. 4) is sufficient by itself to reduce the level of differential rotation on similar time-scales, so that the existence of unstable modes, although important, is not required to achieve rotational recoupling in these high layers.

Model H2 (dashed line in Fig. 4), differing from model H1 only by a smaller rate of spherical-radial differential rotation,  $\partial \ln \Omega / \partial \ln r = -1$ , shows that our conclusions on the stability and transport properties of diffusive magnetorotational modes do not strongly depend on the exact level of differential rotation assumed to be present.

Finally, for completeness, let us mention that, by enforcing  $B_p=0$ , we have been able to identify purely hydrodynamical multi-diffusive (GSF) modes in high-atmospheric layers. These modes were characterized by systematically lower momentum transport efficiencies than their magnetized counterparts. They did not exist in lower atmospheric layers, probably because local conditions are less double-diffusive as one approaches the burning layers (see Table 1). This result is consistent with the findings of Menou et al. (2004): a weak magnetic field acts as a catalyst for rotational instability in a multi-diffusive context, much like it does in an adiabatic context.

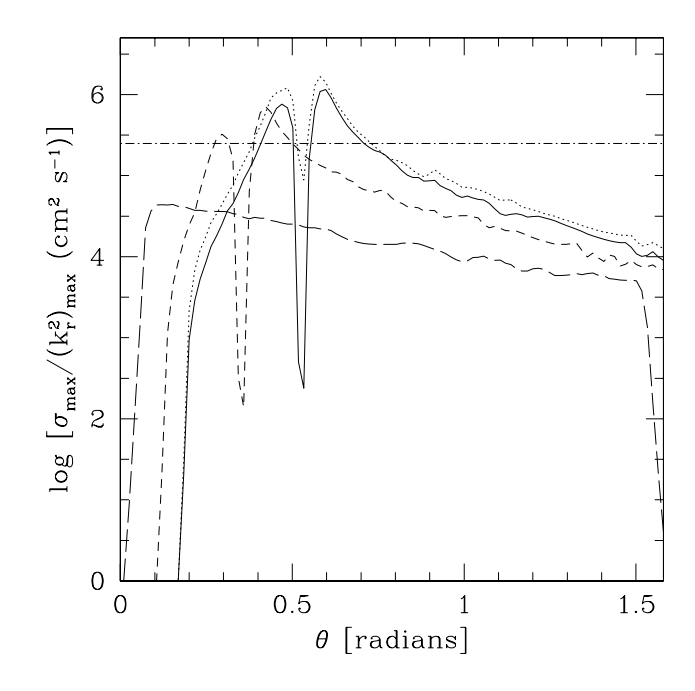
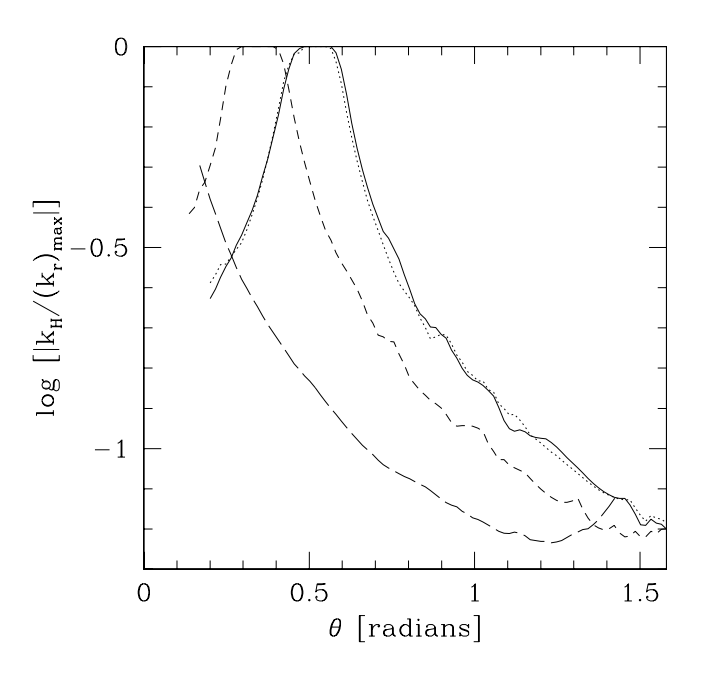


Figure 5. Estimate of the efficiency of spherical-radial momentum transport for typical conditions in a middle-atmospheric layer, as a function of polar angle,  $\theta$ . The solid, dotted, long-dashed and short-dashed lines correspond to models M1, M4, M2 and M3 in Table 2, respectively. The horizontal dash-dotted line indicates the efficiency required to affect the rotation profile over a local scale-height in 1 s.



**Figure 6.** Ratio of spherical-radial wavelength to local scale height, noted  $|k_{\rm H}/k_{\rm r}|$ , for the fastest-growing modes in a middle atmospheric layer, as a function of polar angle,  $\theta$ . Notation is identical to Fig. 5, for the same four models (M1: solid; M2: long-dashed; M3: short-dashed; M4: dotted).

### 3.3 Middle Atmosphere

Having identified important differences between unstable modes in burning and high-atmospheric layers, it is only natural to wonder what would the properties of these modes be in intermediate middle-atmosphere conditions. Figure 5 shows estimated efficiencies of momentum transport, based on fastest-growing linear mode properties, in four different models for middle-atmospheric conditions. The solid, dotted, long-dashed and short-dashed lines correspond to models M1, M4, M3 and M2 in Table 2, respectively. The horizontal dash-dotted line shows the typical efficiency required to affect rotation profiles over a local scale height in 1 s. Figure 6 shows, for the same four models (and same notation as in figure 5), the ratio of the spherical-radial wavelength of the fastest-growing mode to the local scale height, noted  $|k_H/k_r|$ .

Results for middle-atmospheric layers shown in figures 5 and 6 are indeed consistent with the conclusions reached for burning and high-atmospheric layers. In all three models with a misaligned dipole (M1, M3 and M4; Table 2), the effect of the magnetic field geometry is readily seen. In the vicinity of the magnetic "pole," fastest-growing diffusive magneto-rotational modes are characterized by preferentially spherical-radial displacements (nearly along field lines), with a radial wavelength reaching the maximum value,  $l_{\text{max}} \sim H$  (Fig. 6), because the weak magnetic field assumption is not ideally satisfied even for these middleatmospheric conditions. As a result, the modes left unstable in the vicinity of the magnetic pole, which marginally satisfy the constraint on  $l_{\text{max}}$ , have slower growth rates and reduced efficiencies of momentum transport. This is the origin of the dips in figure 5 and plateaus in figure 6, at  $\theta \sim \theta_{\rm mis}$ . The model with an aligned dipole, on the other hand, is characterized by fastest-growing modes with smaller radial wavelengths and transport efficiencies.

What makes middle-atmospheric layers interesting is that, in the models with a misaligned magnetic dipole, estimated efficiencies of momentum transport are in excess of the reference value indicated by the horizontal dash-dotted line, in the vicinity of  $\theta \sim \theta_{\rm mis}$ . These estimates are also much in excess of the transport caused by microscopic viscosity in these layers ( $\nu_{\rm tot} = \nu + \nu_r \sim 3 \times 10^3 \text{ cm}^2 \text{ s}^{-1}$ ; Table 1). Consequently, the influence of these diffusive magneto-rotational modes is expected to dominate the rotational evolution of middle-atmospheric layers, on short enough timescales to possibly have observational consequences. This conclusion is not very sensitive to the exact value of the neutron star angular velocity,  $\Omega$ . A comparison between models M1 and M4 (solid and dotted lines in Fig. 5) shows that a faster stellar rotation leads to faster growth and transport, but only moderately so.

### 4 DISCUSSION AND CONCLUSION

The atmospheres of weakly-magnetized neutron stars are subject to vertical differential rotation during thermonuclear X-ray bursts. Conditions in these atmospheres are also strongly multi-diffusive and thus favor the development of magneto-rotational instabilities. We have presented a linear stability analysis of the expected differential rotation,

with respect to local axisymmetric MHD perturbations, in three representative atmospheric layers. Unstable diffusive magneto-rotational modes were identified in much of the differentially-rotating atmosphere. This indicates that momentum transport between the various atmospheric layers could occur.

Our main motivation to perform a stability analysis is the possibility that the transport resulting from instabilities may have observational consequences for millisecond burst oscillations and associated frequency drifts seen so far in a dozen accreting neutron star systems (nuclear-powered Xray pulsars; e.g. Strohmayer & Bildsten 2003). The differential rotation established during thermonuclear X-ray bursts is transient, lasting perhaps several tens of seconds (a typical burst duration). Therefore, it is not sufficient to identify magneto-rotational instabilities in this context. For these instabilities to have any effect, they must act to modify atmospheric rotation profiles on short enough timescales. We have attempted to address this issue by using linear estimates of the efficiency of momentum transport and have concluded that, indeed, these instabilities could be efficient enough to be of relevance to the bust oscillation phenomenon.

There are reasons to believe that diffusive magnetorotational instabilities will, in a stellar context, tend to reduce the level of existing differential rotation and perhaps make the system approach a state of solid body rotation (see discussion in Menou et al. 2004; see also Korycansky 1991). If correct, this conjecture would have interesting consequences for the coherence of burst oscillations. Indeed, it was noted by Cumming & Bildsten (2000) that the strong coherence of some burst oscillations implies, in the absence of any momentum transport between atmospheric shells, that the feature at the origin of the oscillations must be confined to a surprisingly thin layer (much thinner than a local scale height in their burning layer scenario). This feature would otherwise be smeared out by differential rotation and the oscillations would lose their coherence.

If, however, magneto-rotational instabilities act to reduce the amount of differential rotation present during bursts, as we have suggested, they would effectively promote the coherence of burst oscillations. Constraints on the thickness of the layer from which the modulated signal originates would then be relaxed. Magneto-rotational instabilities would also contribute to the observed frequency drifts of burst oscillations if they act efficiently enough to modify the rotational evolution of atmospheric layers. This possibility is consistent with the results of Cumming et al. (2002), who concluded that conservation of specific angular momentum cannot account for the largest observed frequency drifts.

As attractive as it is, this scenario suffers from a number of significant uncertainties. For instance, we have cautioned about the risks of estimating efficiencies of momentum transport from linear mode properties only. Also, the feature which is at the origin of burst oscillations must be non-axisymmetric. The assumption of axisymmetry made in our analysis could therefore be a limitation. We have illustrated how the properties of fastest growing magnetorotational modes strongly depend on the local magnetic field geometry. This may be viewed as a model uncertainty because the global field topology on a given neutron star is a priori unknown. On the other hand, this sensitivity to magnetic field geometry might in principle be related to the

link recently established between the phases of persistent and burst oscillations, because it suggests a special role for magnetic polar caps in the burst oscillation phenomenon (Chakrabarty et al. 2003; Strohmayer et al. 2003). One then wonders whether the diversity in drift timescales could be attributed to different field geometries in different systems, perhaps caused by varying degrees of field burying under continuous accretion (Cumming, Zweibel & Bildsten 2001).

Another possible limitation of our work comes from neglecting the stabilizing role of composition gradients. In the vicinity of burning layers, substantial composition gradients may be expected in ashes, following the main episode of nuclear burning. The stratification due to composition gradients is important because, contrary to thermal stratification, it is not sensitive to a fast rate of heat transfer. Although it is difficult to assess the importance of stabilization due to composition gradients without a detailed study, the specific example described by Goldreich & Schubert (1967), for a purely hydrodynamical situation, suggests that this effect should be included when discussing neutron star atmosphere during bursts. Another motivation to elucidate the role of stabilizing composition gradients is the possibility that nonaxisymmetric versions of diffusive magneto-rotational modes could contribute to the friction term entering the burning front models of Spitkovsky et al. (2002).

Rather than focusing on burning layers only, we have performed stability analyses at various heights in the differentially-rotating neutron star atmosphere. One motivation for this is the stabilizing effect of composition gradients that we have just discussed. Even if such stabilization occurs in the vicinity of burning layers, magneto-rotational instabilities may still be able to operate higher-up in the atmosphere. A second motivation is the indication, from the work of Cumming et al. (2002; see, e.g., their figure 4), that layers above the burning regions are involved in the burst oscillation phenomenon, since they are the only ones having the right amount of rotational offset to explain the largest observed frequency drifts.

Our analysis for high atmospheric layers shows that magneto-rotational instabilities cease gradually to exist as one approaches the stellar photosphere, because the weak magnetic tension they require becomes increasingly difficult to satisfy. Still, according to our middle-atmospheric models, there is a region above the burning layers in which magnetorotational instabilities can operate and possibly lead to a rather efficient transport of momentum. While burst oscillations have traditionally been associated with burning layers, it may be worth giving more attention to these middleatmospheric layers. Not only do they have the right amount of rotational offset to explain large frequency drifts, but these layers are also more advantageous for the visibility of oscillations, with a short heat diffusion time compared to the time they take to revolve around the star (see Cumming & Bildsten 2000 for a discussion of the visibility of burst oscillations).

We note that Cumming & Bildsten (2000) and Cumming et al. (2002) have invoked the mechanism of magnetic field wind-up described by Spruit (1999) as a possible source of recoupling between differentially-rotating layers. In regions with weak enough stratification from composition gradients for magneto-rotational instabilities to operate, this process may not be relevant. Indeed, in the case

of differentially-rotating accretion disks, it has been argued analytically and demonstrated numerically that the linear growth of the azimuthal field component caused by differential rotation is not important because of the exponential growth of magneto-rotational modes (Balbus & Hawley 1991; 1998). By analogy, one may expect the same linear growth to be irrelevant in the stellar context, given the existence of exponentially-growing diffusive magneto-rotational modes.

Beyond simple qualitative points, it is difficult to deepen an interpretation of burst oscillations and associated frequency drifts in terms of a rotational evolution which is partly driven by magneto-rotational instabilities. A timedependent model for the coupled thermal, chemical and rotational evolution of a neutron star atmosphere during burst seems to be required to make more definite predictions. Such time-dependent models, ignoring the rotational evolution, already exist and exhibit complex behaviors. For example, transient convection early in the burst leads to some mixing of momentum and elements, while inverted composition gradients (which would presumably promote instabilities) are sometimes obtained after the main nuclear burning phase (see, e.g., Woosley & Weaver 1984; Woosley et al. 2003). In order to include the rotational evolution, these models would require reliable estimates of the efficiency of momentum transport (and of the resulting chemical mixing), which could presumably be obtained from fully turbulent numerical simulations of the non-linear development of diffusive magneto-rotational instabilities. Until such advanced tools are developed, it is likely that observations will remain our best guide for understanding burst oscillations and associated frequency drifts.

### ACKNOWLEDGMENTS

It is a pleasure to thank James Cho and Andrew Cumming for useful discussions, Steve Balbus and Lars Bildsten for comments on an early version of the manuscript, and the Department of Astronomy at the University of Virginia for their hospitality.

### REFERENCES

Balbus, S. A. & Hawley, J. F. 1991, ApJ, 376, 214

Balbus, S. A. & Hawley, J. F. 1998, Rev. Mod. Phys., 70, 1

Balbus, S. A. 1995, ApJ, 453, 380

Bildsten, L. 1998, in The Many Faces of Neutron Stars, eds R. Buccheri, J. van Paradijs, and M. A. Alpar. (Dordrecht; Boston: Kluwer Academic Publishers), p. 419

Bildsten, L. 2000, in Cosmic Explosions, Proceedings of the 10th Annual October Astrophysics Conference (AIP Conference Proceedings, Vol. 522), eds. S.S. Holt and W. W. Zhang, p. 359

Chakrabarty, D. et al. 2003, Nature, 424, 42

Cumming, A. et al. 2002, ApJ, 564, 343

Cumming, A. & Bildsten, L. 2000, ApJ, 544, 453

Cumming, A., Zweibel, E. & Bildsten, L. 2001, ApJ, 557, 958

Fricke, K. 1968, Z. Ap., 68, 137

Galloway, D. K. et al. 2003, ApJ, in press, astro-ph/0308122

Goldreich, P. & Schubert, G. 1967, ApJ, 150, 571

Heyl, J. 2003, ApJ, in press, astro-ph/0108450  $\,$ 

Korycansky, D. G. 1991, ApJ, 381, 515

- Lee, U. 2003, astro-ph/0309764
- Lewin, W. H. G., van Paradijs, J. & Taam R. 1995, in X-Ray Binaries, eds. W. Lewin et al. (Cambridge: CUP), p. 175
- Menou, K., Balbus, S. & Spruit, H. 2004, ApJ, in press (astro-ph/0402150).
- Pedlosky, J. 1987, 'Geophysical Fluid Dynamics' (2nd Edition, Springer-Verlag, New York)
- Press, W. H., Teukolsky, S. A., Vetterling, W.T. & Flannery, B. P. 1992, Numerical Recipes in Fortran. The art of scientific computing (Cambridge: Cambridge University Press)
- Ruderman, M. 2003, to appear in X-ray and  $\gamma$ -ray Astrophysics of Galactic Sources, astro-ph/0311228
- Schwarzschild, M. 1958, Structure and Evolution of the Stars (New York: Dover)
- Spitkovsky, A., Levin, Y. & Ushomirsky, G. 2002, ApJ, 566, 1018 Spitzer, L. 1962, Physics of Fully Ionized Gases (New York: Wiley Interscience)
- Spruit, H. C. 1999, A&A, 349, 189
- Strohmayer, T. E. et al. 1996, ApJ, 469, L9
- Strohmayer, T. E. et al. 1997, ApJ, 486, 355
- Strohmayer, T. E. et al. 2003, ApJ, 596, L67
- Strohmayer, T. E. & Bildsten, L. 2003, to appear in Compact Stellar X-Ray Sources, eds. W.H.G. Lewin and M. van der Klis (Cambridge: CUP), astro-ph/0301544
- Tassoul, J.-L. 1978, Theory of Rotating Stars (Princeton: Princeton University Press)
- Woosley, S.E. & Weaver, T.A. 1984, in 'High Energy Transients in Astrophysics' (AIP: Santa Cruz), p. 273
- Woosley, S.E. et al. 2003, ApJ, submitted (astro-ph/0307425)